e-ISSN: 2582-5208
International Research Journal of Modernization in Engineering Technology and Science
( Peer-Reviewed, Open Access, Fully Refereed International Journal )
Volume:07/Issue:01/January-2025 Impact Factor- 8.187 www.irjmets.com

# NUMERICAL SIMULATION OF HEAT TRANSFER OF NANOFLUIDS FLOW IN PLAIN FIN

**Masoud Hatami Garousi*1, Peyman Norouzi*2, Latifeh Arazipoor*3, Narges Fathali*4**

*1Department Of Engineering For Industrial Systems And Technologies, University Of Parma, 43124 Parma, Italy.

*2Faculty Of Mechanical Engineering, Istanbul Technical University, Istanbul, Turkey.

*3Department Of Civil Engineering, Chemistry And Environmental, University Of Genova, Genova, Italy.

*4Department Of Food And Drug, University Of Parma, Parma, Italy.

DOI : https://www.doi.org/10.56726/IRJMETS65901

## ABSTRACT

This paper evaluates the heat transfer and flow dynamics of aluminum oxide ($Al_2O_3$)-water nanofluids within a plain fin heat exchanger, focusing on nanoparticle volume fractions ranging from 0% to 0.8%. The analysis demonstrates that the Nusselt number increases significantly with both nanoparticle concentration and Reynolds number. Specifically, at a Reynolds number of 314, the Nusselt number for a nanofluid with 0.8% volume fraction is 24% higher than that of the base fluid, while at a Reynolds number of 2130, this enhancement decreases to 18%, indicating a diminishing relative benefit at higher turbulence levels. Concurrently, the friction factor exhibits a consistent 46% increase across both low and high Reynolds numbers for the 0.8% volume fraction. Despite the rise in flow resistance, the overall performance evaluation metric (JF-factor) improves substantially, showing a 30% enhancement at low Reynolds numbers and a 36% improvement at high Reynolds numbers. These findings highlight the thermohydraulic advantages of nanofluids, providing a pathway for the development of more energy-efficient thermal systems.

**Keywords**: Nanofluids, Heat Transfer Enhancement, Plain Fin Heat Exchanger, Aluminum Oxide Nanoparticles, Friction Factor

## I. INTRODUCTION

Fin heat exchangers play a key role in thermal management systems by improving heat transfer through increased surface area exposure to the working fluid. Recent research highlights innovations in fin designs, such as combining vortex generators and slit fins, to break up boundary layers and boost heat transfer efficiency. Additionally, using nanofluids—especially hybrid ones like $Fe_3O_4$ and Ag, further improves heat transfer due to their excellent thermal properties and flow behavior. Combining advanced fin designs with these nanofluids offers a promising solution for making heat exchangers more efficient in energy-intensive applications.

Heat transfer and thermal management are critical in advancing electronics and energy systems. Ali et al. [1] demonstrated a 60% improvement in Nusselt number and reduced thermal resistance in microchannel heat sinks using $Al_2O_3$ nanofluids and zigzag fins, emphasizing their potential for electronics cooling. Their study highlighted the importance of fin geometry in inducing secondary flows and improving thermal efficiency. Midhun et al. [2] further explored these systems by optimizing solid–solid phase change material (SSPCM) composite-based plate-fin heat sinks, achieving enhanced electronic thermal management by adjusting parameters like fin count, thermal conductivity enhancers, and heat generation rates. These findings underscored the SSPCM system's capability to maintain electronic device temperatures within critical limits. Gholizadeh et al. [3] highlighted the role of hybrid nanofluids and nonlinear fin arrangements in waste heat recovery applications. By employing Ag and $Fe_3O_4$ nanofluids, they achieved a 7% reduction in exhaust temperatures and demonstrated enhanced thermal performance. Similarly, Ahmed et al. [4] reviewed vortex generators (VGs) and nanofluids, revealing their synergistic effects on compact heat exchanger performance. This comprehensive review emphasized significant thermal performance improvements and energy efficiency gains through optimized VG designs and nanofluid integration. Mousavi et al. [5] utilized AI-driven optimization techniques to design helical-finned double-pipe heat exchangers. By coupling Artificial Neural Networks (ANNs) and Genetic Algorithms (GAs), they demonstrated a 143% improvement in the performance evaluation

criterion (PEC), emphasizing the potential of AI in achieving energy-efficient designs. Studies have also focused on natural convection and forced convection systems. Ravnik et al. [6] analyzed nanofluid-based natural convection scenarios using a three-dimensional Boundary Element Method (BEM), achieving enhanced thermal performance in conduction-dominated flows. Their simulations explored various configurations, including differentially heated cavities and hot strips. In forced convection systems, T'Joen et al. [7] and Wang et al. [8] evaluated inclined louvered fins and fin-and-tube heat exchangers, respectively. T'Joen et al. highlighted the interaction between mean flow and thermo-hydraulic behavior, while Wang et al. developed predictive correlations for optimizing geometric parameters like fin pitch and louver angle. Zakeri et al. [9] demonstrated the impact of $Al_2O_3$-water nanofluids in laminar pipe flows, achieving significant heat transfer enhancements with increasing nanoparticle concentrations and Peclet numbers. Advanced designs and hybrid systems have been extensively investigated to further enhance thermal performance. Zainal et al. [10] studied hybrid nanofluids (Ag/HEG+water) in turbulent forced convection systems, identifying unique thermophysical trends such as increasing Reynolds number enhancing heat transfer but reducing performance at higher nanoparticle concentrations. Azmi et al. [11] conducted experiments on $SiO_2$ nanofluids, identifying an optimal nanoparticle concentration for maximizing Nusselt number without significant frictional losses. Ahmad et al. [12] compared nanofluids in rectangular channels, demonstrating that $SiO_2$-water exhibited the best velocity and pressure drop performance, making it ideal for efficient thermal management systems. Tao et al. [13] achieved an 87% higher Nusselt number in slit-fin heat exchangers compared to conventional designs, attributing the improvement to enhanced synergy between velocity and temperature gradients. Further innovations include He et al. [14] exploration of plain plate fin-and-tube heat exchangers, where reducing the intersection angle between velocity and temperature gradients optimized heat transfer. Huisseune et al. [15] integrated delta winglet vortex generators into louvered fin heat exchangers, significantly improving thermal performance while managing pressure drops. Gavtash et al. [16] simulated cylindrical heat pipes with nanofluids, showcasing reduced thermal resistance and enhanced performance with increased nanoparticle concentrations. Nebbati and Kadja [17] focused on $\gamma$-$Al_2O_3$-water nanofluids in microchannel heat sinks, demonstrating superior cooling efficiency with temperature-dependent thermophysical models and Reynolds number optimization. This comprehensive body of research underscores the advancements in nanofluid technologies, innovative geometries, and AI-driven optimization techniques. These developments have driven the evolution of highly efficient thermal management systems, providing critical insights for future applications in electronics, energy systems, and industrial processes. Wu et al. [18] conducted a numerical simulation to analyze the heat transfer and fluid flow characteristics of composite fins combining longitudinal vortex generators (LVGs) and slit fins. The study revealed that the composite fin achieved 77-90% higher Nusselt numbers compared to plain fins and improved overall performance by 26-50%. Using field synergy and entrance dissipation principles, they demonstrated reduced thermal resistance and enhanced heat transfer efficiency. These results highlight the advantages of innovative composite designs for heat exchanger applications. Fallahzade et al. [19-21] investigated the thermal and hydraulic performance of heat exchangers using advanced optimization techniques under various operational conditions. The study employed numerical simulations to demonstrate the potential of innovative geometries and enhanced working fluids in reducing energy losses and improving heat transfer. These results provide a basis for integrating nanofluids to further optimize heat transfer systems.

Wu et al. [18] demonstrated the potential of composite fins in significantly enhancing heat transfer efficiency, paving the way for innovative heat exchanger designs. Building on this foundation, this paper explores the integration of hybrid nanofluids with plain fins (Fig.1) to further enhance thermal and hydraulic performance. The novelty lies in combining advanced fin geometries with the superior thermophysical properties of hybrid nanofluids, offering a synergistic approach for improved energy efficiency in heat exchangers.

e-ISSN: 2582-5208
International Research Journal of Modernization in Engineering Technology and Science
( Peer-Reviewed, Open Access, Fully Refereed International Journal )
Volume:07/Issue:01/January-2025 Impact Factor- 8.187 www.irjmets.com

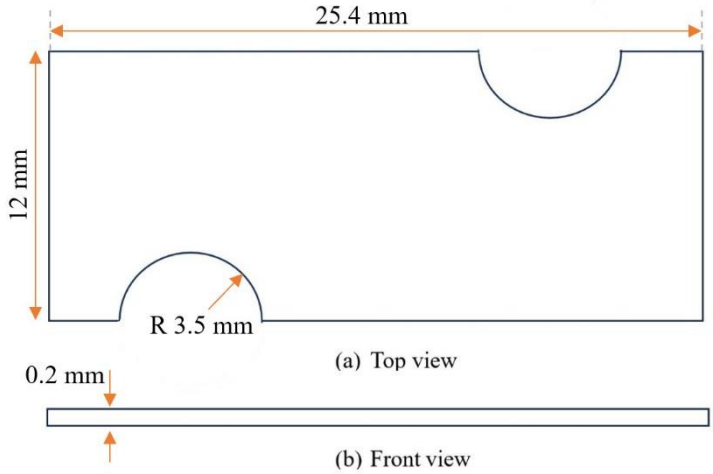


**Fig. 1.** Plain fin dimensions.

## 1. Physical and mathematical model

In this paper, the nanofluid is introduced as the working fluid to enhance heat transfer properties within the composite fin heat exchanger. The nanofluid is modeled as a homogeneous single-phase fluid, assuming uniform dispersion of nanoparticles without relative motion to the base fluid. The thermophysical properties, including density, specific heat, thermal conductivity, and dynamic viscosity, are calculated based on the nanofluid's volume fraction using well-established correlations. Thermophysical properties of water as base fluid and aluminum oxide are present in Table.1.

**Table .** The thermophysical properties of water and aluminum oxide nanoparticles at a temperature of 310 K.

| | Density $(\frac{Kg}{m^3})$ | Specific Heat Capacity $(^{j}/_{kg.K})$ | Thermal conductivity $(^{W}/_{m.k})$ | Dynamic Viscosity (pa.s) |
|---|---|---|---|---|
| $Al_2O_3$ | 3970 | 765 | 40 | - |
| $H_2o$ | 997.1 | 4178 | 0.628 | 0.000695 |
| Al | 2700 | 900 | 220 | - |
| Cu | 8933 | 385 | 400 | - |

### 1.1. Physical model and computational domain

The computational domain for this study mirrors the staggered arrangement of tubes and fins described in the Wu et al. [18]. Adjustments were made to include nanofluid flow, and periodic boundary conditions were applied to reflect real-world scenarios. The heat transfer surface was modeled with constant tube wall temperature, simulating realistic operational conditions.

### 1.2. Governing equations and boundary conditions

The governing equations used in this study are based on the continuity, momentum, and energy equations for three-dimensional, incompressible, steady-state flow which are presented as:

$$\frac{\partial(\rho u_i)}{\partial x_i} = 0 \tag{1}$$

$$\frac{\partial p}{\partial x_k} + \frac{\partial y}{\partial x_i}(\rho u_i u_k) - \frac{\partial}{\partial x_i}\left(\mu \frac{\partial u_k}{\partial x_i}\right) = 0 \tag{2}$$

$$\frac{\partial y}{\partial x_i}(\rho u_i T) = \frac{\partial}{\partial x_i}\left(\frac{\lambda}{C_p}\frac{\partial T}{\partial x_i}\right) \tag{3}$$

e-ISSN: 2582-5208
International Research Journal of Modernization in Engineering Technology and Science
( Peer-Reviewed, Open Access, Fully Refereed International Journal )
Volume:07/Issue:01/January-2025 Impact Factor- 8.187 www.irjmets.com

Modifications were made to include the specific heat and dynamic viscosity of the nanofluid. The density of the nanofluid is computed as:

$$\rho_{nf} = (1-\phi)\rho_f + \phi\rho_s \quad (4)$$

where $\phi$ is the nanoparticle volume fraction, $\rho_{nf}$ is the nanoparticle density, $\rho_f$ is the base fluid density and $\rho_s$ is the nano particle density. Specific heat capacity of the nanofluid can be express as:

$$(\rho C_p)_{nf} = (1-\phi)(\rho C_p)_f + \phi(\rho C_p)_s \quad (5)$$

The thermal conductivity also could be express as:

$$\frac{k_{nf}}{k_f} = \frac{(k_s + 2k_f) - 2\phi(k_f - k_s)}{(k_s + 2k_f) + \phi(k_f - k_s)} \quad (6)$$

Finaly, the dynamic viscosity can be shown as:

$$\mu_{nf} = \frac{\mu_f}{(1-\phi)^{2.5}} \quad (7)$$

These equations are specifically applicable for spherical nanoparticles and assume negligible interparticle interactions.

A nanofluid volume fraction range from 0.2% to 0.8% was employed, with corresponding Reynolds numbers calculated to maintain laminar flow regimes. Based on the equation 4 to equation 7 and using the values provided in Table.1, the density, specific heat, thermal conductivity, and viscosity of the nanofluid were calculated for volume fractions of 0%, 0.2%, 0.4%, 0.6%, and 0.8%. These values are presented in Table.2.

**Table2 .** Thermophysical properties of nanofluid at different volume fractions

| | $\phi = 0\%$ | $\phi = 0.2\%$ | $\phi = 0.4\%$ | $\phi = 0.6\%$ | $\phi = 0.8\%$ |
|---|---|---|---|---|---|
| Density $(\frac{Kg}{m^3})$ | 997.1 | 1003.0458 | 1008.9916 | 1014.9374 | 1020.8832 |
| Specific Heat Capacity $(^{j}/_{kg.K})$ | 4178 | 4150.98 | 4124.284 | 4097.898 | 4071.820 |
| Thermal conductivity $(^{w}/_{m.k})$ | 0.628 | 0.6316 | 0.6352 | 0.6388 | 0.6424 |
| Dynamic Viscosity (pa.s) | 0.000695 | 0.0006984 | 0.0007019 | 0.0007055 | 0.0007090 |

The computational domain incorporates two rows of tubes surrounded by plain fins. The inlet boundary condition specifies a uniform velocity profile with a constant temperature of 308 K. and based on the data on Table.2, the values of inlet velocity for different Reynolds numbers have been calculated. The values for inlet velocity in different Reynold numbers and volume fractions are shown in Table.3.

**Table3 .** Calculation of inlet velocity at different volume fractions

| Re | $\phi = 0\%$ | $\phi = 0.2\%$ | $\phi = 0.4\%$ | $\phi = 0.6\%$ | $\phi = 0.8\%$ |
|---|---|---|---|---|---|
| 314 | 0.03126 | 0.031 | 0.0312 | 0.0311 | 0.03115 |
| 616 | 0.06133 | 0.061 | 0.0612 | 0.0611 | 0.06111 |
| 918 | 0.09140 | 0.091 | 0.0912 | 0.0911 | 0.09107 |
| 1220 | 0.01214 | 0.121 | 0.01212 | 0.1211 | 0.1210 |

e-ISSN: 2582-5208
International Research Journal of Modernization in Engineering Technology and Science
( Peer-Reviewed, Open Access, Fully Refereed International Journal )
Volume:07/Issue:01/January-2025 Impact Factor- 8.187 www.irjmets.com

| | | | | | |
|---|---|---|---|---|---|
| 1521 | 0.1514 | 0.151 | 0.1511 | 0.1510 | 0.1509 |
| 1824 | 0.1816 | 0.181 | 0.1812 | 0.1811 | 0.1809 |
| 2130 | 0.2120 | 0.211 | 0.2116 | 0.2115 | 0.2113 |

The outlet is defined using an outflow condition, assuming negligible backflow. The tube walls are maintained at a constant temperature of 318 K, and symmetry and periodic boundary conditions are applied to lateral boundaries to imitate infinite fin arrays. It should be mentioned that in this study, we have assumed that at the inlet, the velocity profile is uniform and reaches a constant value at the solid surface. Therefore, for the purpose of limited solution simulation, the inlet and outlet regions of the fin were considered to be 1.5 and 9 times the fin length, respectively. The simulations are performed in ANSYS Fluent 18 using the SIMPLE algorithm to couple velocity and pressure fields. The schematic view of the boundary conditions is shown in Fig.2.

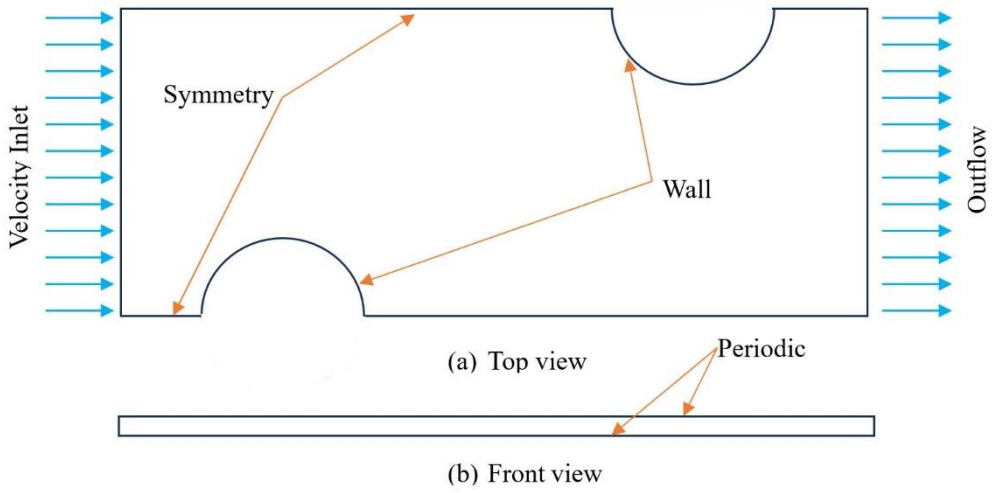


**Fig. 2.** Boundary conditions of the plain fin.

The computational grid is generated using the hexahedral meshing method in ANSYS ICEM CFD. Grid independence is ensured by testing 3 different configurations. The elements number are 4885737 (Case3), 882514 (Case2) and 2132611(Case1) at $Re_{Dc}$ = 1521 based on the tube outside diameter. Based on this numbers for elements, the value of pressure drops along the longitudinal direction of the domain calculated and compared with the results of Wu et al. [18]. Finaly the grid of 882514 is used for further computation in the current investigation. The results of three sets of grid number are listed in Fig.3.

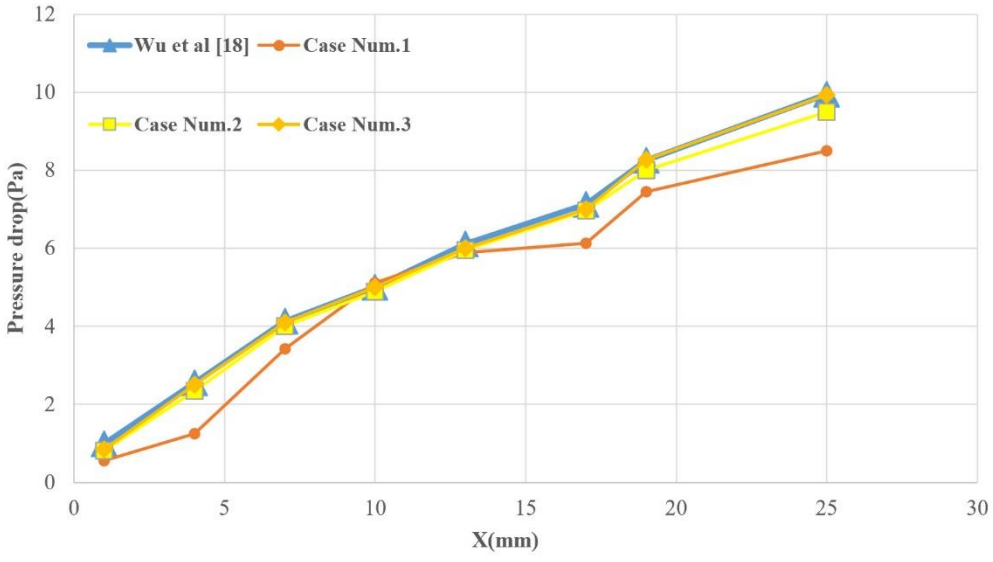


**Fig. 3.** Pressure drops for different mesh configurations.

e-ISSN: 2582-5208
International Research Journal of Modernization in Engineering Technology and Science
( Peer-Reviewed, Open Access, Fully Refereed International Journal )
Volume:07/Issue:01/January-2025 Impact Factor- 8.187 www.irjmets.com

The governing equations are discretized using a second-order upwind scheme for momentum and energy equations and the central difference scheme for diffusion terms. Convergence criteria are set with residuals for velocity components and continuity equations below and energy equations below. Boundary layer grids are employed near solid surfaces to resolve steep gradients in velocity and temperature. Initial conditions are defined based on inlet parameters, and the solution is iterated until numerical convergence is achieved, typically within 5000 iterations. This numerical framework enables a detailed analysis of nanofluid-enhanced plain fins, providing insights into the interplay between fin geometry, fluid dynamics, and heat transfer under various operational conditions.

## II. PARAMETER DEFINITION

To analyze the performance of the nanofluid-enhanced composite fin heat exchanger, key dimensionless parameters are defined for evaluating heat transfer and flow characteristics. These include the Reynolds number ($Re$), Nusselt number ($Nu$), and friction factor(f). The Reynolds number, based on the hydraulic diameter, is calculated as:

$$Re = \frac{\rho u_m D_c}{\mu} \tag{8}$$

where ρ is the nanofluid density, $u_m$ is the mean velocity, $D_c$ is the outer diameter of the tube, and $\mu$ is the nanofluid dynamic viscosity. The Nusselt number is used to evaluate the convective heat transfer performance and is expressed as:

$$Nu = \frac{hD_c}{k} \tag{9}$$

where h is the heat transfer coefficient, and k is the thermal conductivity of the nanofluid. The heat transfer coefficient is defined as:

$$h = \frac{q}{A_0 \Delta T} \tag{10}$$

$$\Delta T = \frac{T_{max} - T_{min}}{log\left(T_{max}/T_{min}\right)} \tag{11}$$

$$T_{max} = max(T_{in} - T, T_{out} - T_w) \tag{12}$$

$$T_{min} = min(T_{in} - T_w, T_{out} - T) \tag{13}$$

where $q$ is the heat flux, $A$ is the heat transfer area, $\Delta T$ is the log mean temperature difference, $T_w$ is the wall temperature, $T_{in}$ is the inlet fluid temperature, and $T_{out}$ is the outlet fluid temperature.

The friction factor ($f$) is calculated as:

$$f = \frac{\Delta P}{\frac{1}{2}\rho u_m^2} \cdot \frac{D_c}{L} \tag{14}$$

$$\Delta P = P_{in} - P_{out} \tag{15}$$

In this relation, ΔP represents the pressure drop, L is the length of the fin corresponds to the direction of flow, $P_{in}$ is the pressure at the inlet, and $P_{out}$ is the pressure at the outlet. It is important to note that the inlet and outlet pressures must be calculated as static pressures.

The Colburn factor is essentially a relation that connects the Nusselt number, Reynolds number, and Prandtl number. It is expressed through Equation 16.

e-ISSN: 2582-5208
International Research Journal of Modernization in Engineering Technology and Science
( Peer-Reviewed, Open Access, Fully Refereed International Journal )
Volume:07/Issue:01/January-2025 Impact Factor- 8.187 www.irjmets.com

$$j = \frac{Nu}{RePr^{\frac{1}{3}}} = \frac{hPr^{\frac{2}{3}}}{\rho u_m c_p} \quad (16)$$

where Pr is the Prandtl number, $c_p$ is the specific heat of nanofluid.

## III. NUMERICAL RESULTS AND DISCUSSIONS

The numerical simulations were performed to evaluate the heat transfer and fluid flow characteristics of a plain fin with nanofluids at varying nanoparticle volume fractions. The analysis focused on the impact of nanofluid concentration on the overall thermal performance of the system, including Nusselt number, friction factor, and overall performance of the system. The Nu number at various Re number range from 304 to 2130 are shown in Fig.4.

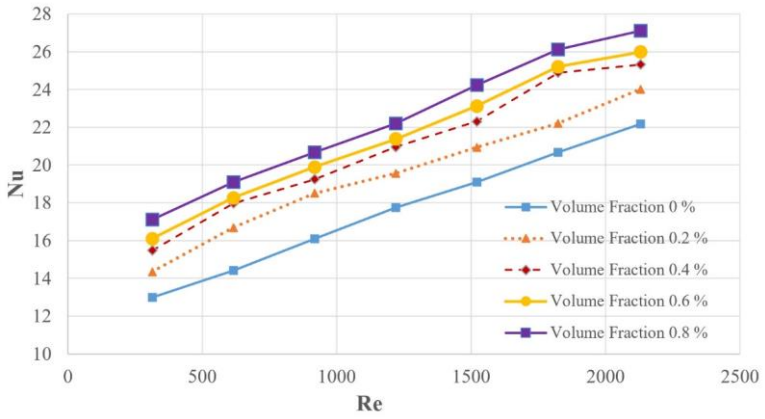


**Fig. 4.** Variations of Nusselt number versus Reynolds number for different volume fractions.

The chart shows the variation of the Nusselt number (Nu) with the Reynolds number (Re) for nanofluids with nanoparticle volume fractions of 0%, 0.2%, 0.4%, 0.6%, and 0.8% used with a plain fin. As the Reynolds number increases, the Nusselt number rises linearly across all cases, indicating improved convective heat transfer at higher flow rates. At a low Reynolds number of 314, the Nusselt number for a volume fraction of 0.8% is 24% higher than that for 0%, demonstrating a significant enhancement in heat transfer. However, at higher Reynolds numbers of 2130, this difference reduces to 18%, suggesting that the relative benefit of nanofluids diminishes slightly as turbulence increases. Overall, the chart highlights the influence of nanofluid concentration and flow conditions, with higher volume fractions and lower Re showing greater proportional improvements. The friction factor f at various Re number range from 304 to 2130 are shown in Fig. 5.

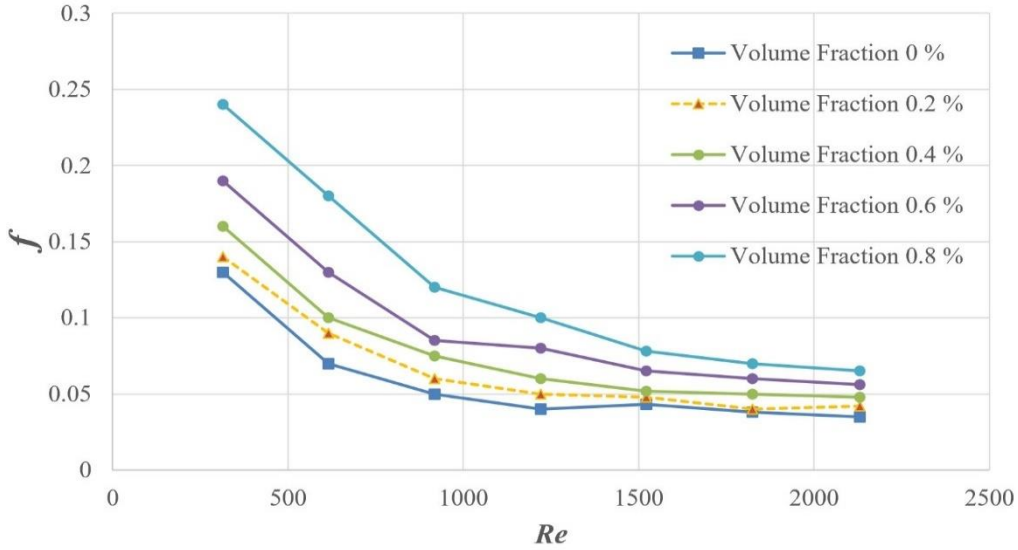


**Fig. 5.** Friction factor f

e-ISSN: 2582-5208
International Research Journal of Modernization in Engineering Technology and Science
( Peer-Reviewed, Open Access, Fully Refereed International Journal )
Volume:07/Issue:01/January-2025 Impact Factor- 8.187 www.irjmets.com

The chart illustrates the variation of the friction factor ($f$) with the Reynolds number ($Re$) for nanofluids with nanoparticle volume fractions of 0%, 0.2%, 0.4%, 0.6%, and 0.8% in a plain fin system. As the Reynolds number increases, the friction factor decreases across all cases, consistent with typical flow behavior in laminar and transitional regimes. At a low Reynolds number of 314, the friction factor for a volume fraction of 0.8% is 46% higher than that for 0%, and this same 46% difference is observed at the high Reynolds number of 2130. This demonstrates that the relative impact of nanoparticle concentration on flow resistance remains consistent across different flow conditions. The chart highlights the trade-off between heat transfer enhancement and consistent increases in flow resistance when using nanofluids. To evaluate the impact of nanofluid volume fractions on the performance of a plain fin, temperature contours were analyzed for various volume fractions. Fig.6 presents the static temperature distributions for volume fractions of 0.2 and 0.4.

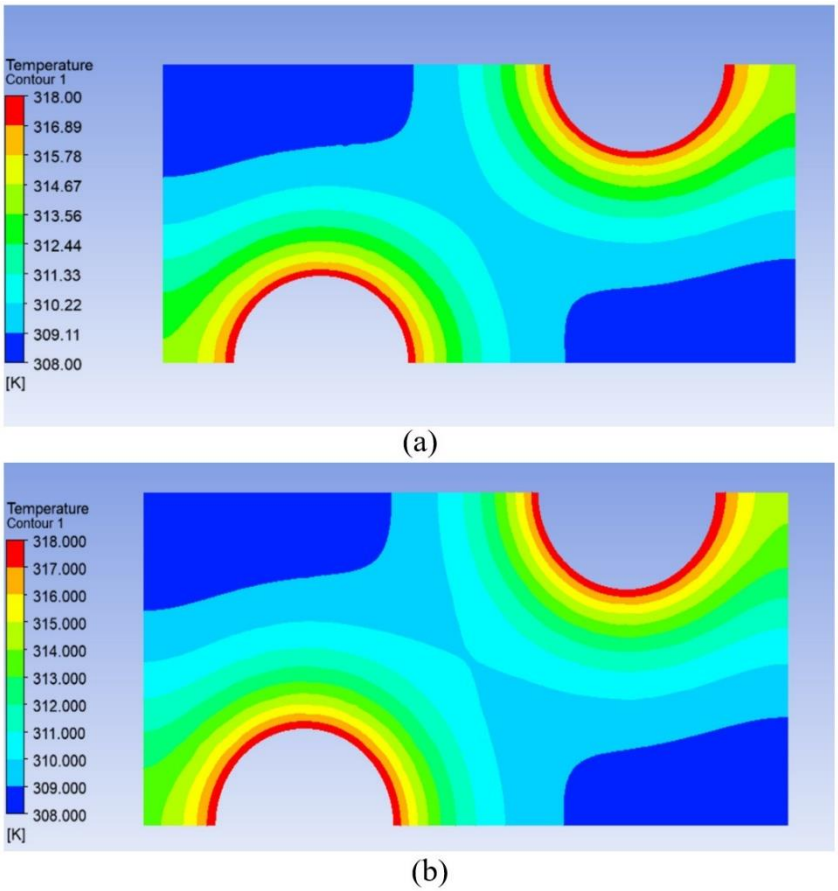


**Fig. 6.** Temperature contour for Volume fractions, (a) 0.4, (b) 0.2

Fig.6 illustrates the temperature contours for nanofluid volume fractions of 0.4 and 0.2, highlighting the thermal behavior of a plain fin under different conditions. The contours reveal that the temperature decreases radially outward from the heated surface, as shown by the gradient from red to blue. With a volume fraction of 0.4, the higher thermal conductivity of the nanofluid results in a more uniform temperature distribution. In contrast, at a lower volume fraction of 0.2, the reduced thermal conductivity leads to a steeper temperature gradient near the heated zones. This demonstrates how varying nanofluid volume fractions influence the heat transfer efficiency and overall temperature distribution of the fin.

The JF factor, represented by the ratio $\frac{J}{f^{1/3}}$, serves as a metric for assessing the overall performance of the fin [18] and is illustrated in Fig.7.

e-ISSN: 2582-5208
International Research Journal of Modernization in Engineering Technology and Science
( Peer-Reviewed, Open Access, Fully Refereed International Journal )
Volume:07/Issue:01/January-2025 Impact Factor- 8.187 www.irjmets.com

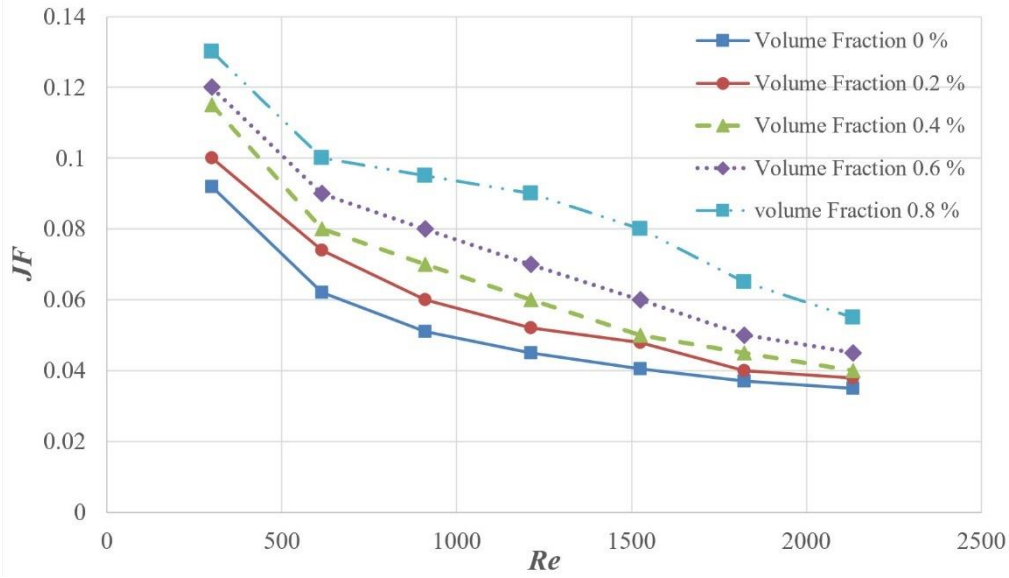


**Fig. 7.** Overall performance in different filling ratios.

The chart depicts the variation of the *J F* -factor with Reynolds number for nanofluids with nanoparticle volume fractions of 0%, 0.2%, 0.4%, 0.6%, and 0.8% in a plain fin system. The *J F* -factor decreases as the Reynolds number increases, reflecting the combined effects of reduced Colburn and friction factors at higher flow rates. At a low Reynolds number of 314, the *J F* -factor for a 0.8% volume fraction is 30% higher than that for 0%, while at a high Reynolds number of 2130, this difference increases to 36%, highlighting the growing benefit of nanofluids at higher turbulence. For a given Reynolds number, higher nanoparticle volume fractions consistently exhibit increased *J F* -factors due to enhanced heat transfer performance. The highest *J F* -factor is observed at a 0.8% volume fraction, demonstrating the optimal balance between heat transfer enhancement and flow resistance, emphasizing the role of nanofluids in boosting thermal-hydraulic performance.

## IV. CONCLUSION

The investigation underscores the transformative potential of nanofluids in enhancing the thermohydraulic performance of plain fin heat exchangers. The substitution of the base fluid with $Al_2O_3$-water nanofluids results in marked improvements in heat transfer, as evidenced by increases in the Nusselt number. For a Reynolds number of 314, a 0.8% nanoparticle volume fraction yields a 24% higher Nusselt number compared to the base fluid, while this enhancement decreases to 18% at a Reynolds number of 2130, reflecting a reduced impact at higher turbulence levels. The consistent 46% rise in the friction factor for the 0.8% volume fraction highlights the trade-off between heat transfer improvement and increased flow resistance. However, the overall performance evaluation criterion (JF-factor) demonstrates significant benefits, with enhancements of 30% and 36% at low and high Reynolds numbers, respectively. These results emphasize the efficacy of nanofluids in optimizing thermal system performance. Future research should explore hybrid nanofluids, advanced fin geometries, and real-time optimization techniques to further refine the thermodynamic and hydraulic performance of heat exchanger systems.

## V. REFERENCES

[1] Ali, A. M., Angelino, M., & Rona, A. (2021). Numerical analysis on the thermal performance of microchannel heat sinks with Al2O3 nanofluid and various fins. Applied Thermal Engineering, 198, 117458.

[2] Midhun, V. C., Maroliya, M., & Saha, S. K. (2024). Numerical investigation and optimisation of solid–solid phase change material composite-based plate-fin heat sink for thermal management of electronic package. Applied Thermal Engineering, 248, 123183.

[3] Gholizadeh, A., Pourfallah, M., Gholinia, M., Armin, M., & Languri, E. (2022). The role of nanofluids and fins in a heat exchanger on waste energy recovery from a diesel engine: An experimental and numerical study. Energy Reports, 8, 13353-13368.

[4] Ahmed, H. E., Mohammed, H. A., & Yusoff, M. Z. (2012). An overview on heat transfer augmentation using vortex generators and nanofluids: approaches and applications. Renewable and Sustainable Energy Reviews, 16(8), 5951-5993.

[5] Mousavi, S. M., Azizi, A. S., Razbin, M., Darzi, A. A. R., & Li, M. (2025). Optimized design of helical-finned double pipe heat exchangers via numerical simulation and artificial intelligence. Applied Thermal Engineering, 258, 124605.

[6] Ravnik, J., Škerget, L., & Hriberšek, M. (2010). Analysis of three-dimensional natural convection of nanofluids by BEM. Engineering Analysis with Boundary Elements, 34(12), 1018-1030.

[7] T'Joen, C., Huisseune, H., Canière, H., Steeman, H. J., Willockx, A., & De Paepe, M. (2011). Interaction between mean flow and thermo-hydraulic behaviour in inclined louvered fins. International Journal of Heat and Mass Transfer, 54(4), 826-837.

[8] Wang, C. C., Lee, C. J., Chang, C. T., & Lin, S. P. (1999). Heat transfer and friction correlation for compact louvered fin-and-tube heat exchangers. International journal of heat and mass transfer, 42(11), 1945-1956.

[9] Zakeri, M., Barati, S., & Davarnejad, R. (2013). Simulation of convective heat transfer of a nanofluid in a circular cross-section. International Journal of Engineering, 26(6), 571-576.

[10] Tan, C., Zainal, S., Sian, C. J., & Siang, T. J. (2016). ANSYS simulation for Ag/HEG hybrid nanofluid in turbulent circular pipe. Journal of Advanced Research in Applied Mechanics, 23(1), 20-35.

[11] Azmi, W. H., Sharma, K. V., Sarma, P. K., Mamat, R., Anuar, S., & Rao, V. D. (2013). Experimental determination of turbulent forced convection heat transfer and friction factor with SiO2 nanofluid. Experimental Thermal and Fluid Science, 51, 103-111.

[12] Ahmad, U. K., Hasreen, M., Yahaya, N. A., & Rosnadiah, B. (2017). Comparative study of heat transfer and friction factor characteristics of nanofluids in rectangular channel. Procedia engineering, 170, 541-546.

[13] Tao, W. Q., Cheng, Y. P., & Lee, T. S. (2007). 3D numerical simulation on fluid flow and heat transfer characteristics in multistage heat exchanger with slit fins. Heat and Mass Transfer, 44, 125-136.

[14] He, Y. L., Tao, W. Q., Song, F. Q., & Zhang, W. (2005). Three-dimensional numerical study of heat transfer characteristics of plain plate fin-and-tube heat exchangers from view point of field synergy principle. International Journal of Heat and Fluid Flow, 26(3), 459-473.

[15] Huisseune, H., T'joen, C., De Jaeger, P., Ameel, B., De Schampheleire, S., & De Paepe, M. (2013). Performance enhancement of a louvered fin heat exchanger by using delta winglet vortex generators. International Journal of Heat and Mass Transfer, 56(1-2), 475-487.

[16] Gavtash, B., Hussain, K., Layeghi, M., & Lafmejani, S. S. (2012). Numerical simulation of the effects of nanofluid on a heat pipe thermal performance. International Journal of Mechanical and Mechatronics Engineering, 6(8), 1462-1468.

[17] Nebbati, R., & Kadja, M. (2015). Study of forced convection of a nanofluid used as a heat carrier in a microchannel heat sink. Energy Procedia, 74, 633-642.

[18] Wu, X., Zhang, W., Gou, Q., Luo, Z., & Lu, Y. (2014). Numerical simulation of heat transfer and fluid flow characteristics of composite fin. International Journal of Heat and Mass Transfer, 75, 414-424.

[19] Fallahzadeh, R., Garousi, M. H., Pagliarini, L., Bozzoli, F., & Cattani, L. (2024). Single-Loop Triple-Diameter Pulsating Heat Pipes at Reduced Heat Input: A CFD Study on Inner Diameter Optimization. Energies, 17(22), 5568.

[20] Casoli, P., Vescovini, C. M., Masoud, H. G., & Rundo, M. (2024). A Novel 1D Approach for Modelling Gas Bladder Suppressors on the Delivery Line of Positive Displacement Pumps. Energies, 17(7), 1610.

[21] Garousi, M. H., Karimi, M., Casoli, P., Rundo, M., & Fallahzadeh, R. (2024). Vibration Analysis of a Centrifugal Pump with Healthy and Defective Impellers and Fault Detection Using Multi-Layer Perceptron. Eng, 5(4), 2511-2530.